Near-Body Shadowing Analysis at 60 GHz

Theodoros Mavridis, Luca Petrillo, Julien Sarrazin, *Member, IEEE* Aziz Benlarbi-Delaï, Philippe De Doncker

***Abstract*—A numerical model of the fading of a receiver located near the user body at 60 GHz in an indoor environment is presented. The model is based on the indoor channel model IEEE 802.11ad. The results are presented for a receiver located in a zone from 5 to 30 cm away from the body. With the shadowing depending on the region (front or back) with respect to the base station, the mean attenuation of the channel over the bandwidth is analyzed and model thanks to a Two-Wave Diffuse Power distribution model.**

***Index Terms*—Body Area Networks, Millimeter waves, 60 GHz, Creeping wave, V-Band, Near-Body, Fading**

I. Introduction

The popularity of wireless communication technologies has increased the need for reliable, high-speed communications. Successive technologies have been proposed using large bands of the RF spectrum. The next emerging technologies for achieving short-range indoor communications with data rates of a few Gbit/s are foreseen to work at 60 GHz [1]. The progress in low-cost mm-wave circuit design and the wide available spectrum around 60 GHz will allow for developing new communication services such as HD streaming video, augmented reality, wireless gaming, Gigabit Ethernet,... [2].

However, millimeter-wave propagation introduces high path losses and fading effects. One of the most important interaction to deal with is the human body influence on the communication channel. In this context, 60 GHz Body Area Networks (BANs) [3] have been studied in order to characterize the path loss for both on- [4], [5] and off-body [6], [7] scenarios. More particularly, [8] has studied the effect of clothes on the on-body path loss. Some research have also focused on the development of efficient antennas for body centric applications [9]. More recently, statistical models of fading have also been proposed for dynamic on-body situations [10], [11].

Also, some works have studied the shadowing created by a body blocking the main path [12]. However, one of the most probable scenarios would be the presence of the human body next to the communication device. The widespread of smartphones and tablets has increased the need for higher wireless data rates in a close region around the human body (against the ear, in front of the user,...). We choose to define a new spatial region from 5 to 30 cm away from the body, referred to as the *Near-Body* zone. This zone corresponds to the region where the user often places his smartphone, tablet or laptop.

T. Mavridis, L. Petrillo and P. De Doncker are with OPERA Dpt. - Wireless Communications Group, Université Libre de Bruxelles (ULB), B-1050 Brussels, Belgium e-mail: (tmavridi@ulb.ac.be ; lpetrillo@ulb.ac.be ; pdedonck@ulb.ac.be)

T. Mavridis, J. Sarrazin and A. Benlarbi-Delaï are with Sorbonne Universités, UPMC Univ Paris 06, UR2, L2E, F-75005, Paris, France e-mail: (julien.sarrazin@upmc.fr; aziz.benlarbi_delai@umpc.fr)

In this paper, a simple diffraction model is proposed for a receiver located from 5 to 30 cm away from the body. The model is similar to deterministic BAN channel models [6], [13]. The simplicity of the model does not allow an exact description of the channel since it does not take into account complex interactions such as arm movements, etc. However, the model is able to spatially characterize the channel around the human body and to give a physical understanding of the phenomenon.

Section II presents the numerical implementation of the indoor off-body channel model. General considerations about the model, the spatial region under study and the simulations are also presented. Then, Section III studies the mean attenuation of the channel over the bandwidth in this Near-Body scenario. Also, a discussion of the communications aspects is given. Section IV presents the experimental validation. Finally, section V concludes this paper.

II. Indoor Near Body Channel Implementation

In [6], an off-body channel model has been derived by modeling the human body by a circular cylinder. The cylindrical model has been widely used in the literature [14] and it is convenient to model static (or averaged) scenario. [4] showed that the electric properties of the body model can be set to the human skin. Also, in [8], the impact of clothing on 60 GHz on-body propagation has been studied and no significant impacts on path loss have been observed. At 60 GHz, the cylindrical model has been investigated experimentally and

it was shown that the cylindrical model gives a maximum 3 dB error on the electric field power measured on a real human torso-body [6]. In the following, we will consider that this error is small enough to consider a cylindrical model for the human body in static scenarios.

However, in [6], the antenna was always assumed to be at maximum 5 mm from the human body. Using the same methodology, a modified model can be derived for larger distances from 5 to 30 cm. This will model the channel between an external base station and a user using a device close to his body. The developed model is ray-based so that it can be included in Saleh-Valenzuela like channel models [15].

A. Geometry and Spatial Regions

The base station and the user are located in an indoor environment. The user holds a communication device close to him in the small zone drawn in Fig. 1.

It is proposed to split space into two regions with respect to the transmitter (Tx): front and back as presented in Fig. 2. The regions are defined azimuthally with respect to the human body model (cylinder).

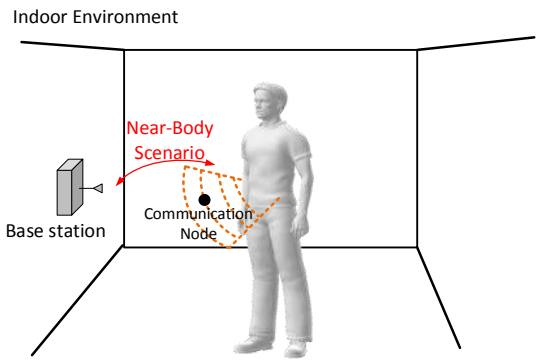

Fig. 1. Schema of the scenario.

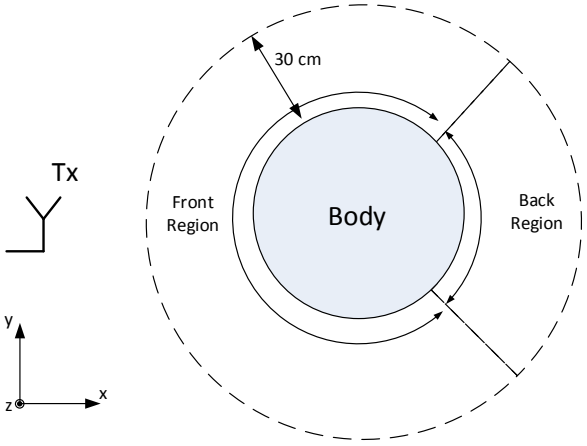

Fig. 2. Studied Regions Scheme with respect to the transmitter (Tx).

The regions are defined by considering the location of the receiving antenna in regards of the fixed base station and the body location. The front region is then defined as the set of points where the base station and the receiving antenna are in line-of-sight while the locus given by the non-line-of-sight configurations is the back region. It is worth noticing that this definition is then not related to the real orientation of the user.

This definition of the front and back regions are in agreement with the physical regions in [6]: lit and shadow region which had been defined by considering the behaviour of the electric field (Geometrical Optics and creeping wave).

In the simulations in section III, the base station and the human body are moved randomly in the indoor environment but the definition of the regions still remains as described above.

B. Diffraction Model

The diffraction model in the front (or lit) region is calculated using Geometrical Optics (GO). These solutions are trivial and not presented here but can be found in [16].

In [6], the classic modal solution of the scattering by a circular cylinder is derived in the back (or shadow) region into a creeping wave formulation using Watson's transform. It is known that the modal solution has convergence issues while the creeping wave formulation in (1) is a fast computing and convergent solution.

In [13], due to the close-to-cylinder assumption, the sum was approximated to the first creeping wave mode. For distances between 5 cm and 30 cm, it can be numerically shown that three terms of (1) are enough to obtain an acceptable accuracy.

For a normalized incident plane wave transmitted by a vertically polarized antenna and called TM, the creeping wave modes formulation is given by [13]:

$$\begin{aligned}
E_\rho^{\text{tot,TM}} &= -2\pi j\cos\theta_i e^{jkz\cos\theta_i}\sum_l j^{\upsilon_l}\tilde{a}_\tau H_{\upsilon_l}^{(2)'}(k\rho\sin\theta_i)\Phi_{\upsilon_l}(\phi)\\
E_\phi^{\text{tot,TM}} &= 2\pi\frac{\cot\theta_i}{jk\rho}e^{jkz\cos\theta_i}\sum_l \upsilon_l j^{\upsilon_l-1}\tilde{a}_\tau H_{\upsilon_l}^{(2)}(k\rho\sin\theta_i)\Phi_{\upsilon_l}(\phi)\\
E_z^{\text{tot,TM}} &= 2\pi\sin\theta_i e^{jkz\cos\theta_i}\sum_l j^{\upsilon_l}\tilde{a}_\tau H_{\upsilon_l}^{(2)}(k\rho\sin\theta_i)\Phi_{\upsilon_l}(\phi)
\end{aligned} \tag{1}$$

where k is the free space wavenumber, θ_i is the elevation angle of the incident plane wave and

$$\tilde{a}_\tau = \frac{1}{m}\frac{A'(\tau)-qA(\tau)}{\tau W_2(\tau)-qW_2'(\tau)}, \tag{2}$$

$\upsilon_l = ka+m\tau_l$, $m=(ka/2)^{1/3}$, $\Phi_\upsilon(\phi)=\frac{\cos\upsilon(\phi-\pi)}{\sin\pi\upsilon}$ and $q=m\sqrt{\varepsilon_r}$. ε_r is the complex relative permittivity, a is the cylinder radius and ρ is the distance between the center of the cylinder and observation point. In these equations, $H_\upsilon^{(2)}$ is the Hankel function and A, W_2 are respectively the standard and modified Airy functions [6]. The τ_l are obtained by solving:

$$W_2'(\tau_l)-qW_2(\tau_l)=0. \tag{3}$$

For a normalized TE incident plane wave, the creeping wave modes formulation is calculated by:

$$\begin{aligned}
E_\rho^{\text{tot,TE}} &= -j\frac{1}{k\rho}\frac{e^{-jkz\cos\theta_i}}{\sin\theta_i}2\pi\sum_l \upsilon_l' j^{\upsilon_l'}\tilde{b}_{\tau_l'}H_{\upsilon_l'}^{(2)}(k\rho\sin\theta_i)\Phi_{\upsilon_l'}(\phi)\\
E_\phi^{\text{tot,TE}} &= je^{-jkz\cos\theta_i}\frac{2\pi}{m}\sum_l j^{\upsilon_l'+1}\tilde{b}_{\tau_l'}H_{\upsilon_l'}^{(2)'}(k\rho\sin\theta_i)\Phi_{\upsilon_l'}(\phi)\\
E_z^{\text{tot,TE}} &= 0
\end{aligned} \tag{4}$$

where $\upsilon_l' = ka+m\tau_l'$, τ_l' verifies $W_2'(\tau_l)-qW_2(\tau_l)=0$ and

$$\tilde{b}_\tau = \frac{1}{m}\frac{qA'(\tau)-A(\tau)}{q\tau W_2(\tau)-W_2'(\tau)}, \tag{5}$$

Numerically, it can be shown by comparing the creeping wave modes formulation to the Eigenmode solution [17] that the first three modes are sufficient to reach a maximal 3 dB error between both solutions in the Near-Body region. This error corresponds to the accuracy of the circular cylinder model found in [6].

C. Indoor Channel Implementation

The general structure of the polarized impulse response of the IEEE 802.11ad model can be written as [15]:

$$\mathbf{h}(t,\phi_{\text{Tx}},\theta_{\text{Tx}},\phi_{\text{Rx}},\theta_{\text{Rx}}) = \sum_i \mathbf{H}^{(i)} \times$$
$$C^{(i)}(t-T^{(i)},\phi_{\text{Tx}}-\Phi_{\text{Tx}}^{(i)},\theta_{\text{Tx}}-\Theta_{\text{Tx}}^{(i)},\phi_{\text{Rx}}-\Phi_{\text{Rx}}^{(i)},\theta_{\text{Rx}}-\Theta_{\text{Rx}}^{(i)}) \quad (6)$$

where $C^{(i)}$ is the impulse response relative to the i^{th} cluster:

$$C^{(i)}(t,\phi_{\text{Tx}},\theta_{\text{Tx}},\phi_{\text{Rx}},\theta_{\text{Rx}}) = \sum_k \alpha_{(i,k)}\delta(t-\tau^{(i,k)}) \times$$
$$\delta(\phi_{\text{Tx}}-\phi_{\text{Tx}}^{(i,k)})\delta(\theta_{\text{Tx}}-\theta_{\text{Tx}}^{(i,k)})\delta(\phi_{\text{Rx}}-\phi_{\text{Rx}}^{(i,k)})\delta(\theta_{\text{Rx}}-\theta_{\text{Rx}}^{(i,k)}) \quad (7)$$

where,

- $\mathbf{h}$ is the channel impulse response
- $t, \tau, \phi_{\text{Tx}}, \theta_{\text{Tx}}, \phi_{\text{Rx}}, \theta_{\text{Rx}}$ are, respectively, time, delay, azimuth and elevation angles at the transmitter (Tx) and receiver (Rx).
- $\mathbf{H}^{(i)}$ is the i^{th} 2x2 polarization matrix cluster gain.
- $T^{(i)}, \Phi_{\text{Tx}}^{(i)}, \Theta_{\text{Tx}}^{(i)}, \Phi_{\text{Rx}}^{(i)}, \Theta_{\text{Rx}}^{(i)}$ are the temporal and angular coordinates of i^{th} cluster.
- $\alpha_{(i,k)}$ is the k^{th} ray magnitude of the i^{th} cluster.

In an off-body scenario, each ray in (6)-(7) is perturbed by the presence of the human body near the receiver. In order to extend the model to an off-body scenario, the idea is to convert each ray in (6)-(7) into a wave diffracted by a circular cylinder with a radius a and an antenna located at (ρ, ϕ_0) position. Let $\mathcal{T}$ be the operator applying this transformation:

$$\begin{pmatrix} \alpha^{(i,k)'} \\ \tau^{(i,k)'} \\ \phi_{\text{rx}}^{(i,k)'} \\ \theta_{\text{rx}}^{(i,k)'} \end{pmatrix} = \mathcal{T}_{(a,\rho,\phi_0)} \begin{pmatrix} \alpha^{(i,k)} \\ \tau^{(i,k)} \\ \phi_{\text{rx}}^{(i,k)} \\ \theta_{\text{rx}}^{(i,k)} \end{pmatrix} \quad (8)$$

where the parameters in the off-body scenario take ' and the other parameters on the right-hand side are given by the IEEE 802.11ad model. By using the GO and the equations (1) and (4) developed above, $\mathcal{T}$ can be easily defined in the Near-Body zone by considering the two regions: $\mathcal{T}^{\text{front}}$ in the front region and $\mathcal{T}^{\text{back}}$ in the back one.

The indoor channel model, equations (6) and (7), considered in the following is the *Conference Room* of the IEEE802.11ad and more particularly the AP-AP one [15]. This means that the transmitting and receiving antennas are placed at the same height and are spaced by 2 meters. The cylinder modelling the human body has a 0.2 m radius and it is filled with material equivalent to the human skin ($\varepsilon_r = 7.97 - 10.92j$). The channel is evaluated all around the body (from 0° to 360° in azimuth) with an angular step of 0.3° and from 5 to 30 cm away from it with a radial step of 0.5 mm. Hundred channel realizations using the IEEE are evaluated and injected in the model.

The transmitting antenna is assumed to be TM polarized, i.e. the transmitted electric field is parallel to the body height. The receiver is also assumed to be z-oriented.

In the 60 GHz bandwidth, some communication protocols have been set up such as Wigig [18]. Orthogonal frequency-division multiplexing (OFDM) is considered to achieve communication. Hence, in this paper, it is proposed to study signal shadowing in the Near-Body zone through the mean frequency channel response over the bandwidth which is the relevant parameter describing channel attenuation for OFDM:

$$\mu_H = \frac{1}{\Delta f}\int_{\Delta f} |H(f)| \mathrm{d}f \quad (9)$$

with $H(f)$ the channel frequency response.

At 60 GHz, the antenna aperture can not be neglected and has to be taken into account since the carrier wavelength is 5 mm. In the following, spatial integration of the electric field is performed along on the spatial extension of about the antenna aperture used in the experimental validation, which is 1 mm^2. To highlight the effect of taking into account the size aperture, both cases will be numerically investigated: with and without the spatial integration on the antenna aperture.

III. Mean Attenuation

A. Front Region Distribution

In the front region, the electric field is calculated using Geometrical Optics. The main impact on μ_H is due to the line-of-sight ray and the reflection off the cylinder. The other rays arriving on the body have lower power due to the higher travelled distance. This situation is well suited to be modelled by a Two-Wave Diffuse Power (TWDP) distribution [19] which models the received amplitude V as :

$$V = V_1 e^{j\Phi_1} + V_2 e^{j\Phi_2} + \sum_i \tilde{V}_i e^{j\Phi_i} \quad (10)$$

where $V_{1,2}$ denotes the magnitude of the specular components $1, 2$ and $\Phi_{1,2}$ are the random associated phases. The second part of (10) describes the non-specular components. The probability density function (PDF) of r, the magnitude of V, used to fit the simulation in Fig. 3-4 is calculated by:

$$\text{TWDP PDF}(r;\Delta,K,\sigma) = f(r) = \frac{r}{\sigma^2} e^{\frac{-r^2}{2\sigma^2}-K} \times \frac{1}{\pi}\int_0^\pi e^{\Delta K\cos\theta} I_0\left(\frac{r}{\sigma}\sqrt{2K(1-\Delta\cos\theta)}\right)\mathrm{d}\theta \quad (11)$$

where σ^2 is the variance of the diffuse part, I_0 is the modified Bessel function of the first order, K is equivalent to the Rice factor, $K = \frac{V_1^2+V_2^2}{2\sigma.^2}$, and Δ is defined by:

$$\Delta = \frac{\text{Peak Specular Power}}{\text{Average Specular Power}} - 1 = \frac{2V_1V_2}{V_1^2+V_2^2} \quad (12)$$

It can be easily deduced that the specular magnitudes are given by:

$$V_1 = \frac{\sqrt{K\sigma^2}}{2}\left(\sqrt{2+\Delta}+\sqrt{2-\Delta}\right)$$
$$V_2 = \frac{\sqrt{K\sigma^2}}{2}\left(\sqrt{2+\Delta}-\sqrt{2-\Delta}\right) \quad (13)$$

Fig. 3 shows an example of probability density function and its best fitting.

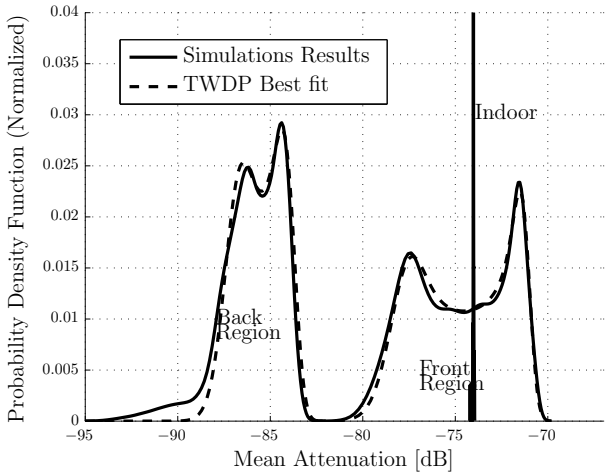

Fig. 3. Probability density functions. Without Antenna Aperture Integration. $K = 21.65$ dB, $\Delta = 0.66$ and $\sigma = 1.25 \times 10^{-5}$ in the front region and $K = 20.85$ dB, $\Delta = 0.35$ and $\sigma = 3.50 \times 10^{-6}$ in the back one. The Indoor distribution corresponds to the case without the body presence.

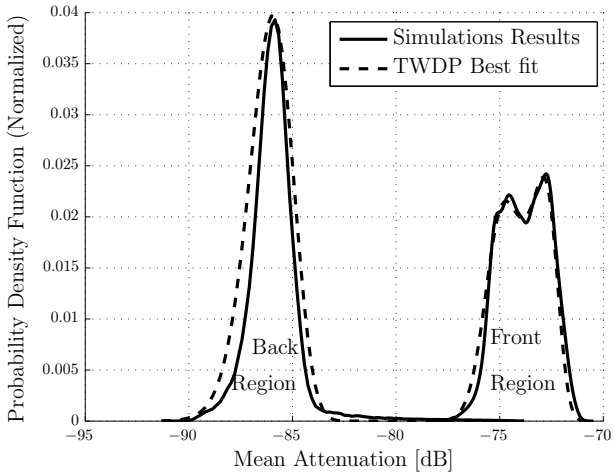

Fig. 4. Probability density functions. With Antenna Aperture Integration. $K = 20.84$ dB, $\Delta = 0.32$ and $\sigma = 1.33 \times 10^{-5}$ in the front region and $K = 15.74$ dB, $\Delta = 0.11$ and $\sigma = 5.79 \times 10^{-6}$ in the back one

To fit the obtained data with a two-wave diffuse power distribution, a Maximum Likelihood (MLE) algorithm was used. However, it has been heuristically observed that the convergence of the algorithm is highly dependent to the initial values of the parameters. An easy way of getting these initial values is using the moments μ_n of the TWDP distribution:

$$\mu_n = \int_0^\infty r^n f(r) \mathrm{d}r \tag{14}$$

It has been shown in [20] that the first moments are:

$$\begin{aligned} \mu_1 &= (1+K)2\sigma^2 \\ \mu_2 &= (2\sigma^2)^2 \frac{1}{2}(4 + 8K + K^2(2+\Delta^2)) \\ \mu_3 &= (2\sigma^2)^3 \frac{1}{2}(12 + 36K + 9K^2(2+\Delta^2) + K^3(2+3\Delta^2)) \end{aligned} \tag{15}$$

TABLE I
TWO-WAVES DIFFUSE POWER PARAMETERS IN THE FRONT REGION. THE VALUES ARE OBTAINED NUMERICALLY ON HUNDRED CHANNEL REALIZATIONS.

Case	Parameter	Mean Value	$CI_{95\%}$
Without Antenna Aperture Int.	K	21.70 dB	[21.04, 22.01] dB
	σ	1.23×10^{-5}	$[1.19, 1.32]\times10^{-5}$
	Δ	0.62	[0.606, 0.627]
	V_1	-73.63 dB	[-73.64, -73.58] dB
	V_2	-89.56 dB	[-89.76, -89.51] dB
With Antenna Aperture Int.	K	20.84 dB	[20.49, 21.12] dB
	σ	1.33×10^{-5}	$[1.29, 1.38]\times10^{-5}$
	Δ	0.32	[0.315, 0.326]
	V_1	-73.71 dB	[-73.72, -73.68] dB
	V_2	-95.48 dB	[-95.69, -95.44] dB

TABLE II
TWO-WAVES DIFFUSE POWER PARAMETERS IN THE BACK REGION. THE VALUES NUMERICALLY ARE OBTAINED ON HUNDRED CHANNEL REALIZATIONS.

Radius	Parameter	Mean Value	$CI_{95\%}$
Without Antenna Aperture Int.	K	13.26 dB	[5.38, 18.56] dB
	σ	8.07×10^{-6}	$[0.41, 1.98]\times10^{-5}$
	Δ	0.13	[0.01, 0.27]
	V_1	-85.94 dB	[-89.47, -82.77] dB
	V_2	-108.7 dB	[-119.71,-97.54] dB
With Antenna Aperture Int.	K	15.74 dB	[8.07, 20.40] dB
	σ	5.79×10^{-6}	$[0.34, 1.31]\times10^{-5}$
	Δ	0.11	[0.01, 0.25]
	V_1	-85.82 dB	[-82.299, -89.290] dB
	V_2	-111.36 dB	[-117.50, -101.82] dB

Solving this system for each channel realization allows one to give initial values for the distribution parameters K, σ and Δ. Hundred simulations have been computed using the model proposed above and the values of K, σ and Δ have been obtained for each one. It has been numerically observed that these parameters can be well described by a normal distribution. For sake of clarity, the mean value and the 95% confidence interval are presented in Table. I. The confidence interval gives typical bounds and is summarized as $CI_{95\%}$.

Since the distribution has high K values, the distribution tends to a two-wave distribution but the TWDP is more suited for this problem. This latter better models the rising and descending parts of the curve drawn in Fig. 3.

B. Back Region Distribution

The back region can also been modeled by a TWDP distribution. The same parameters are calculated from the back region and summarized in table II.

By comparing the results from Tables I and II, it can be

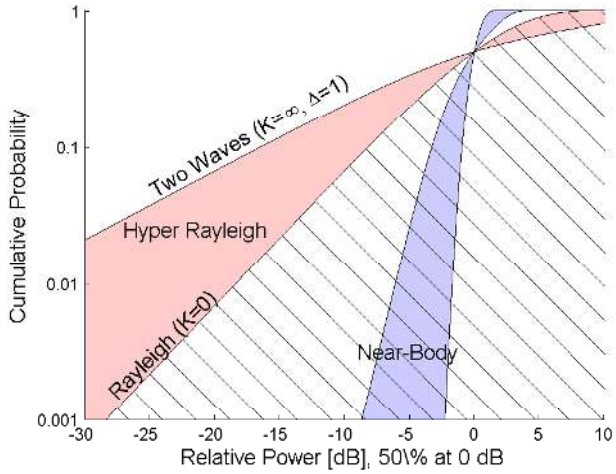

Fig. 5. Cumulative distribution functions representing the hyper Rayleigh region and the Near-Body scenario. The Ricean region corresponds to the hatched one.

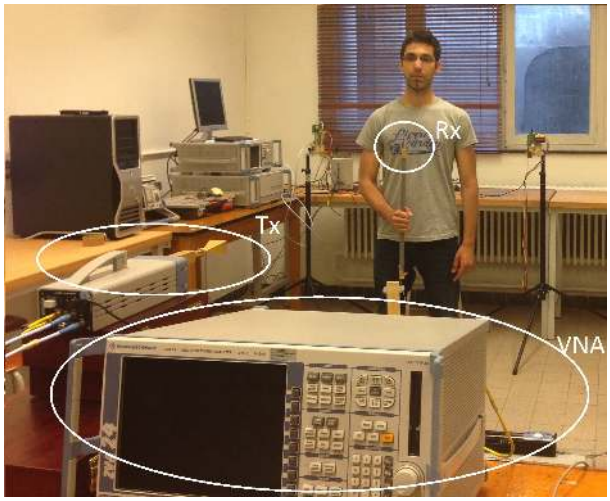

Fig. 6. Photo of the experimental setup.

seen that the antenna integration have a severe impact in the Front Region where Δ goes from 0.6 to 0.3 while in the Back one, the variations are limited. As expected, the attenuation of V_1 and V_2 can be noticed between the front and the back region. The range of variation ($CI_{95\%}$) of the parameters is also wider in the back region which creates higher variability of the obtained distributions.

In the front region, parameters have a low standard deviation. This can be easily explained by the fact that the behaviour of μ_H is only dictated by the direct ray and the reflected one off the body. It seems that the position in the environment have almost no impact on the results and hence, on the fading. On the other hand, the back region is more influenced by the user location since the fitting parameters are more affected.

By comparing the cases with and without antenna integration, it is important to notice that the antenna averages the received power implying a reduction of fading. It seems that the antenna reduces the impact of small scale variations which can be seen by the large reduction of Δ in the front region. In the back region, the two-wave distribution is no longer visible in the probability density function. In summary, it can be inferred that the antenna aperture has a strong smoothing effect on fading.

Recent research [21], [22] has identified and measured the existence of *Hyper-Rayleigh* fading. This term has been introduced to define a fading more severe than the one predicted by the Rayleigh model. It has been empirically shown by [21] that in some specific environments 20% of measurements exhibit *Hyper-Rayleigh* fading. The worst case is obtained in a two-wave environment (TWDP with $\Delta = 1$ and $K = \infty$). Since we defined the Near-Body region with a TWDP distribution, it is necessary to evaluate the type of fading occurring.

Frolik [21] has defined three fading families (Ricean, Rayleigh and Hyper Rayleigh) based on the received power cumulative distribution function (CDF). They are presented in Fig. 5 for the case without antenna aperture integration where the hatched region corresponds to Ricean like fading. The cumulative probabilities have been normalized such that 0 dB corresponds to a 50% probability. The Near-Body region fading has been plotted for the Front Region using the parameters of Table I. The limits of this region are obtained using the parameters in Table I at the first standard deviation. It can be seen that the Near-Body fading is in a deep Ricean region insuring weak fading.

IV. Experimental Comparison

The main experimental parameters are presented in Table III. A collection of 1001 channel acquisition points has been obtained randomly in front of the user body using a *Rohde & Schwarz* Vector Network analyser. To increase the dynamic range a 30 dB amplifier was placed at the receiver side and a 3 dB open waveguide antenna was used at the transmitter side. The user was located at 2 m from the transmitter and the receiver was located randomly from 5 cm to 30 cm away from the user body. The antenna were both located at 1.2 m height. To allow shadowing characterization, an omni-directional antenna (*FLANN Microwave* ref. MD249-AA) has been used at the receiver side. The user holds a support specifically designed for moving the antenna with his hand. This could simulate the utilization of a smart-phone or tablet. In order to compare with the results without the body presence, measurements have been taken with an automatic positioning device during another channel measurement. The room were the measurements have been conducted has a size of 7 m $\times$ 4 m and a height of 2.5 m. The receiver has been placed at the center of the room and the transmitter 2 m away. A photography of the experimental set-up is presented in Fig. 6. The experimental mean attenuation over the bandwidth is shown in Fig. 7.

Fig. 7 shows a TWDP distribution in the front region. The fading seems to be comparable to the simulated results. The

TABLE III
EXPERIMENTER PARAMETERS

Symbol	Value
Center Frequency	60 GHz
Bandwidth	2 GHz
Number of frequency points	501
VNA IFbandwidth	10 kHz
Total Number of channel acquisitions	1001
Body Perimeter	93 cm
Body Height	1.85 m
Body Mass	75 kg

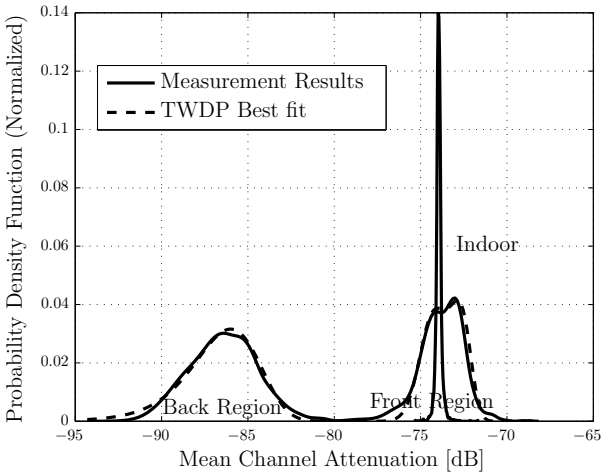

Fig. 7. Measured Probability density functions. The presented fittings are presented in dotted line. The shadowing whithout the body presence is referred to Indoor.

spread of the fading between the indoor case and the front region one is also comparable to previous results. As expected, in the back region, the averaged received power is reduced as compared to the front one.

The fitting parameters are summarized in Table IV. It is more convenient to compare the triple of values (V_1, V_2, σ) since it has a clear physical meaning. In the front region, the experiment results give (-73.49 dB, -96.87 dB, 1.3×10^{-5}) and the simulated values with antenna aperture integration give $(-73.71,\ -95.48,\ 1.33\times10^{-5})$ dB. This shows a maximal absolute error of about 1.5 dB and a maximal relative error of about 1.5 % which shows a good agreement between experiment and simulations.

TABLE IV
EXPERIMENTAL BEST FIT PARAMETERS

	Front Region	Back Region
K	21.24 dB	9.44 dB
σ	$1.3 \cdot 10^{-5}$	$12.79 \cdot 10^{-6}$
Δ	0.27	0.11
V_1	-73.49 dB	-85.42 dB
V_2	-96.87 dB	-116.62 dB

For experimental results, the back region gives the triple (-85.42 dB, -116.62 dB, 1.28×10^{-5}) and (-85.82 dB, -111.36 dB, 5.8×10^{-6}) for the simulations. These values show some differences especially regarding σ. The measured results are in the confidence interval ($CI_{95\%}$) of Table II.

Discrepancies between experiments and simulations point out some weaknesses of the numerical model. Actually, the signal is impacted by small movements of the body (such as trembling, breathing,...) even in a "static" scenario. Also, the body has a more complex geometry than the circular cylinder and therefore, in the simulation results, the reflections off the user body have not been completely taken into account like the arm of the user that moved the antenna.

Since the experiment gives relatively close agreement to the numerical simulations, it can be concluded that the TWDP distribution as presented here is convenient to simulate body shadowing at 60 GHz.

V. CONCLUSION

In this work, the study of the Near-Body region is proposed for 60 GHz communications. This spatial region is extended from 5 to 30 cm away of the user body. This scenario would be relevant when users are using their devices such as smartphones, laptops or tablets. A numerical model based on the indoor channel model standardized by IEEE802.11ad coupled with simple diffraction models has been used. The diffraction model assumes that the human body can be modeled by a circular cylinder. The aim of this model is to quickly characterize the fading close to the body user in static situations.

This Near-Body zone has been split up into two regions: front and back, with respect to the transmitter since the physical phenomena are different. It has been shown that this latter is spatially distributed as a two wave diffuse power distribution (TWDP) for both the front and back regions which models the fading by considering two specular components with diffuse scattered fields. The model has been illustrated in the case of the *Conference Room* of the indoor channel IEEE802.11ad. The mean attenuation of the channel has been spatially studied. The results of the fading are summarized by presenting the mean value and the 95% confidence interval of the three parameters of the TWDP distribution. Between these two regions, the specular components are reduced by about 10 to 15 dB in the back region and the diffuse power is also reduced of about 3 dB. The experiments have shown results fitting into the confidence interval of the simulations, assessing the model.

Also, the worst case of a TWDP has been discussed by introducing the concept of hyper-Rayleigh environments. Nevertheless, it has been shown that the Near-Body fading is in the Ricean-like fading region.

VI. ACKNOWLEDGMENT

This work was performed within the Labex SMART supported by French state funds managed by the ANR within the

Investissements d'Avenir programme under reference ANR-11-IDEX-0004-02. This work is also supported by grants of the FNRS (FRIA grant), Belgium.

REFERENCES

[1] N. Guo, R. C. Qiu, S. Mo, and K. Takahashi, "60-GHz millimeter-wave radio: Principle, technology, and new results," *EURASIP J. Wireless Commun. Netw.*, 2007.

[2] S. K. Yong and C. C. Chong, "An overview of multigigabit wireless through millimeter wave technology: Potentials and technical challenges," *EURASIP J. Wireless Commun. Netw.*, vol. 2007, p. 10 pages, 2006.

[3] A. Pellegrini, A. Brizzi, L. Zhang, K. Ali, Y. Hao, X. Wu, C. Constantinou, Y. Nechayev, P. Hall, N. Chahat, M. Zhadobov, and R. Sauleau, "Antennas and propagation for body-centric wireless communications at millimeter-wave frequencies: A review," *IEEE Antennas Propag. Mag.*, vol. 55, no. 4, pp. 262–287, Aug. 2013.

[4] N. Chahat, G. Valerio, M. Zhadobov, and R. Sauleau, "On-body propagation at 60 ghz," *IEEE Trans. Antennas Propag.*, vol. 61, no. 4, pp. 1876–1888, April 2013.

[5] L. Petrillo, T. Mavridis, J. Sarrazin, D. Lautru, A. Benlarbi-Delaï, and P. De Doncker, "Analytic creeping wave model and measurements for 60 GHz body area networks," *IEEE Trans. Antennas Propag.*, vol. 62, no. 8, pp. 4352–4356, 2014.

[6] T. Mavridis, L. Petrillo, J. Sarrazin, D. Lautru, A. Benlarbi-Delaï, and P. De Doncker, "Theoretical and experimental investigation of a 60 GHz off-body propagation model," *IEEE Trans. Antennas Propag.*, vol. 62, no. 1, pp. 393–402, 2014.

[7] N. Chahat, M. Zhadobov, L. Le Coq, S. I. Alekseev, and R. Sauleau, "Characterization of the interactions between a 60-ghz antenna and the human body in an off-body scenario," *IEEE Trans. Antennas Propag.*, vol. 60, no. 12, pp. 5958–5965, 2012.

[8] A. Guraliuc, M. Zhadobov, G. Valerio, N. Chahat, and R. Sauleau, "Effect of textile on the propagation along the body at 60 GHz," *IEEE Trans. Antennas Propag.*, vol. 62, no. 3, pp. 1489–1494, Mar. 2014.

[9] N. Chahat, M. Zhadobov, and R. Sauleau, "Antennas for body centric wireless communications at millimeter wave frequencies," *In Progress in Compact Antennas, InTech*, pp. 23–55, Sep. 2014.

[10] Y. Nechayev, C. Constantinou, X. Wu, and P. Hall, "De-polarization of on-body channels and polarization diversity at 60 GHz," *IEEE Trans. Antennas Propag.*, vol. PP, no. 99, pp. 1–1, 2014.

[11] L. Petrillo, T. Mavridis, J. Sarrazin, A. Benlarbi-Delaï, and P. De Doncker, "Statistical on-body measurement results at 60 GHz," *IEEE Trans. Antennas Propag.*, vol. 63, no. 1, pp. 400–403, 2014.

[12] C. Gustafson and F. Tufvesson, "Characterization of 60 ghz shadowing by human bodies and simple phantoms," in *6th European Conference on Antennas and Propagation (EUCAP)*. IEEE, 2012, pp. 473–477.

[13] T. Mavridis, L. Petrillo, J. Sarrazin, D. Lautru, A. Benlarbi-Delaï, and P. De Doncker, "Creeping wave model of diffraction of an obliquely incident plane wave by a circular cylinder at 60 GHz," *IEEE Trans. Antennas Propag.*, p. 1, 2014.

[14] A. Fort, C. Desset, P. De Doncker, P. Wambacq, and L. Van Biesen, "An ultra-wideband body area propagation channel model-from statistics to implementation," *IEEE Trans. Microw. Theory Tech.*, vol. 54, pp. 1820–1826, 2006.

[15] A. Maltsev et al, "Channel models for 60 GHz WLAN systems," *IEEE 802.11 TGad document: IEEE 802.11-09/0334r8*, 2010.

[16] Y. A. Kravtsov and N. Zhu, *Theory of Diffraction : Heuristic Approaches*. Alpha Science, 2010.

[17] W. C. Chew, *Waves and Fields in Inhomogeneous Media*. New York: IEEE Press, 1995.

[18] C. Hansen, "Wigig: Multi-gigabit wireless communications in the 60 GHz band." *IEEE Wirel. Commun.*, vol. 18, no. 6, pp. 6 – 7, 2007.

[19] G. D. Durgin, T. S. Rappaport, and D. A. De Wolf, "New analytical models and probability density functions for fading in wireless communications," *IEEE Trans. Commun.*, vol. 50, no. 6, pp. 1005–1015, 2002.

[20] D. Dixit and P. Sahu, "Performance of qam signaling over twdp fading channels," *IEEE Trans. Wirel. Commun.*, vol. 12, no. 4, pp. 1794–1799, April 2013.

[21] J. Frolik, "A case for considering hyper-rayleigh fading channels," *IEEE Transactions on Wireless Communications*, vol. 6, no. 4, pp. 1235–1239, 2007.

[22] ——, "On appropriate models for characterizing hyper-rayleigh fading," *IEEE Transactions on Wireless Communications*, vol. 7, no. 12, pp. 5202–5207, 2008.

Theodoros Mavridis is born in Brussels, Belgium, in 1988. He received his Master degree in physical engineering from the Universit Libre de Bruxelles, Brussels, Belgium, in 2011. In 2011, he joined the OPERA Dpt. - Wireless Communication Group where he began his thesis on the propagation channel for Body Area Networks at 60 GHz and the spatial focusing techniques.

Luca Petrillo graduated in electronic engineering from the University of Genoa, Italy, in 2008. He received the Master's degree in Communication Systems and the Doctoral degree from the University Pierre et Marie Curie, Paris, France, in 2008 and 2011, respectively. From October 2008 to September 2011 he was a researcher at Onera, France. From October 2011 to August 2012 he was an Associate Professor at the University Pierre et Marie Curie, where he taught electronics. Since September 2012 he accomplishes post-doctoral training at the Ecole Polytechnique of Bruxelles, Belgium. His scientific interests are in the field of electromagnetic propagation, including surface wave propagation, periodic structures (metamaterials, EBG), human body propagation in different scenarios, and in electromagnetic systems, including HF radars, Body Area Networks, 60 GHz wireless systems, Green Radio.

Julien Sarrazin received his Master and PhD degrees from the University of Nantes in France, in 2005 and 2008 respectively. In 2009 and 2010, he worked at the BK Birla Institute of Technology of Pilani in India. In 2011 and 2012, he was a research engineer at Telecom ParisTech in Paris. Since September 2012, he is Associate Professor at the University of Pierre and Marie Curie (UPMC) in Paris, where he is currently working in the Electronics and Electromagnetism Lab (L2E) in the field of Body Area Networks (BAN) and 60 GHz communications. His research interests also include antenna design, MIMO systems, wireless communication and localization, propagation channel, metamaterials.

Aziz Benlarbi-Delaï received the PhD in Electrical Engineering and The Habilitation Diriger des Recherches (HDR) s Sciences Physiques from the University of Lille I in 1992 and 2002. From 1992 to 2006 he was Assistant Professor at this University and was involved, as researcher at the Institute of Electronic Microelectronic and Nanotechnology (IEMN), in the field of microwave and microfluidic devices and systems for connected objects, and also in the field of ultra fast sampling using micro and nanostructures. He is currently a full time Professor in Electrical Engineering at the University Pierre et Marie Curie (UPMC Paris 06) and head of the laboratory of Electronics and Electromagnetism (L2E). He is involved in research aiming millimetre wave communication and localization for green radio and intelligent ambient issues.

He is the author of 94 publications and communications and the holder of two patents. He participated to several Technical Program Committees of international conferences and is visiting professor or member of the external evaluation team of several foreign universities.

Philippe De Doncker received the M.Sc. in physics engineering and Ph.D. degrees from the Universit libre de Bruxelles (ULB), Belgium, in 1996 and 2001, respectively. He is currently Professor with the Universit libre de Bruxelles. His research interests focus on wireless communications and electromagnetics.